ATLAS Internal Note
LARG Note - ??

Hadronic Endcap Modules Zero Pion and Electron Energy Scan Analysis from April 1998 Testbeam Data

Matt Dobbs[1], Michel Lefebvre[2], and Dugan O'Neil[3]

University of Victoria,
Victoria, Canada.

September 8, 1998

Abstract

The Hadronic Endcap modules Zero were tested in the H6 beamline at CERN in April 1998. The response and resolution are evaluated at four impact points for electrons and pions over an energy range of 20 to 180 GeV. The response varies within 1% for electrons and 6% for pions over this range. The electron energy resolution is parameterized as $\frac{\sigma}{E} = \frac{22.1\pm\ 0.8\%}{\sqrt{E_0}} \oplus\ 0.4 \pm\ 0.5\% \ \oplus\ \frac{0.55\pm\ 0.07}{E_0}$ where E_0 is expressed in GeV. The pion energy resolution (with pre-subtracted noise) is parameterized as $\frac{\sigma}{E} = \frac{82\pm\ 1\%}{\sqrt{E_0}} \oplus 5.2 \pm\ 0.2\%$ giving an energy resolution of $\frac{\sigma}{E} = 10.6\%$ at 100 GeV.

[1]Matthew.Adam.Dobbs@Cern.CH
[2]Lefebvre@UVic.CA
[3]Dugan@UVic.CA

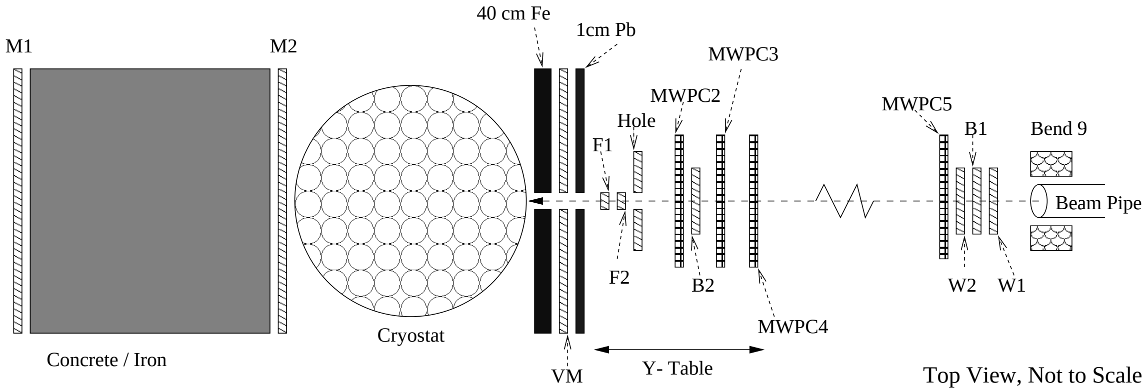

Figure 1: Setup of the HEC testbeam.

1 Introduction

The ATLAS Hadronic Endcap Calorimeter (HEC) is a liquid argon sampling calorimeter with copper absorbers [1]. Prototypes have previously been tested in beams at CERN [2]. The modules Zero are the first HEC modules built to the final ATLAS design specifications and, unlike previous prototypes, contain 10 interaction lengths affecting near full longitudinal containment of hadronic showers. Also, better lateral containment is achieved by these modules than by any previous modules.

One full ATLAS HEC will consist of 32 pie-shaped modules. The readout segmentation will be $2\pi/64$ in ϕ and 0.05-0.1 in pseudorapidity. The modules Zero consist of four phi segments (2 per module) totaling 1/16 of one endcap.

The construction of the ATLAS Hadronic Endcap modules Zero were completed in spring 1998. In April 1998, testbeam data were recorded for pion, electron and muon beams with energies ranging from 20 to 180 GeV. This paper focuses on the energy scans that were performed at several impact positions to assess the energy response and resolution of the calorimeter.

In section 2 an overview of the experimental setup is presented. The data runs are briefly described in section 3. Sections 4 and 5 concentrate on determining the response and resolution of the calorimeter to electrons and pions respectively.

2 Experimental Setup

The modules were installed in the H1 cryostat in the H6 beamline of the SPS at CERN. Trigger counters and multi-wire proportional chambers installed in the beamline (see Figure 1) provide trigger and particle identification information.

Though the Hadronic Endcap is constructed so as to provide a semi-pointing geometry in pseudorapidity, space constraints within the cryostat prevent the modules Zero from being tilted such that beam particles are incident in a pointing manner (see Figure 2). Thereby a hadronic shower will deposit energy in a larger number of cells than it would in a pointing orientation, necessitating the use of larger clusters and increasing the electronic

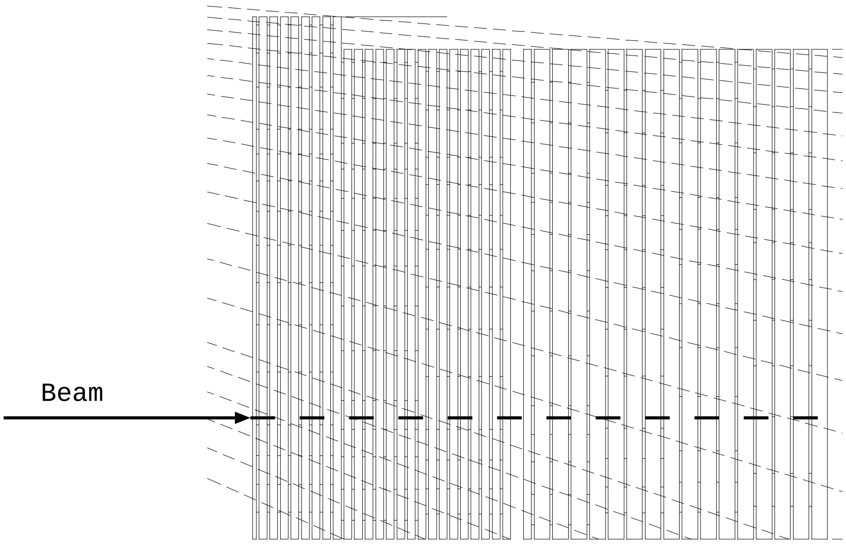

Figure 2: Orientation of the beam with respect to the calorimeter [1, Fig. 8-1]. The thick line represents the incident (non-pointing) particle beam. The thin dashed lines are drawn at constant pseudorapidity from the ATLAS interaction point, such that a particle traveling in a straight line from the vertex would follow this trajectory. The readout cells are positioned in a "semi-pointing" manner which follows these pseudorapidity lines in a stepped fashion.

noise contribution to the energy resolution.

Longitudinally the calorimeter is divided into three readout depths. The first depth ($z = 1$) consists of 8 liquid argon (LAr) gaps each separated by 2.5 cm of copper. The second depth ($z = 2$) consists of 16 LAr gaps also separated by 2.5 cm of copper. The third depth ($z = 3$) consists of 16 gaps each separated by 5 cm of copper. The change in sampling fraction in the third depth necessitates the application of a factor of two relative to the first two depths when reconstructing the energy deposited in this layer.

The two modules Zero are identical with the exception of the high resistive coating which implements the high voltage distribution within the gaps. One module uses a Carbon Loaded Paint (CLP) as a resistive coating, while the other uses a Carbon Loaded Kapton (CLK) resistive coating. In the final ATLAS design the CLK resistive coating will be employed in all modules.

Each LAr gap contains an electrostatic transformer structure which effectively divides the gap into four sub-gaps as shown in Figure 3. During the April 1998 beam period, module 2 suffered from high voltage problems in its third depth, requiring 1 subgap in each of the first 8 gaps to be disconnected from high voltage, while one subgap in each of the second 8 gaps had its high voltage reduced by a factor of $\frac{1}{3}$. As will be shown in the sections to follow, the resolution of module 2 is completely recoverable using energy dependent depth weights.

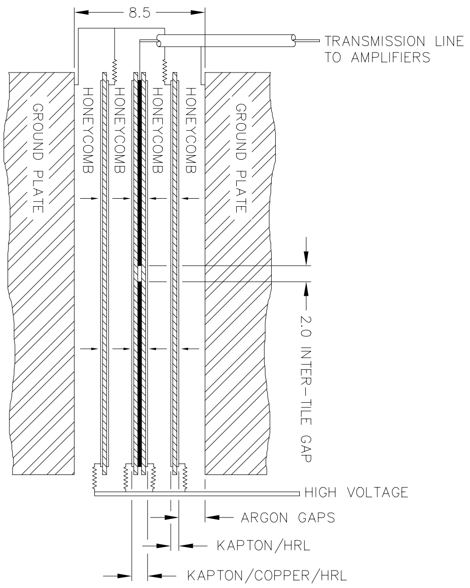

Figure 3: Subgap structure within each LAr gap [1, Fig. 8-4].

3 Data

Energy scans at 4 impact positions for electron and pion beams are analyzed. These positions are labeled D, E, H, & I, and are presented in the table below where x is measured from the center of the cryostat and y is measured from the beam's nominal impact position.

Position	Impact Cell	x (mm)	y (mm)
Module 1			
D	5	-100	+83
H	3	-100	-67
Module 2			
E	78	+100	+83
I	76	+100	-67

Figure 4 shows the geometrical layout of the impact positions.

Impact positions D & E (H & I) belong to different modules but are identical in every other way. Positions D & E differ from positions H & I in that they each contain a tie rod which holds the layers of the calorimeter in place.

Pion data were taken at beam energies of 20, 40, 60, 80, 100, 119.1, and 180 GeV, while electron data were taken at 20, 40, 60, 80, 100, and 119.1 GeV. The run numbers corresponding to these data are tabulated in the Appendix.

Each run consists of 6,000 to 10,000 events (including random triggers and physics events) with the exception of the 20 GeV pion runs which suffered from low rate and contain 1000 to 2000 events.

The signal from each readout cell for each event is recorded every 25 ns for a total of 400 ns providing 16 time slices. Figure 5 shows a typical signal shape. The first 4 time

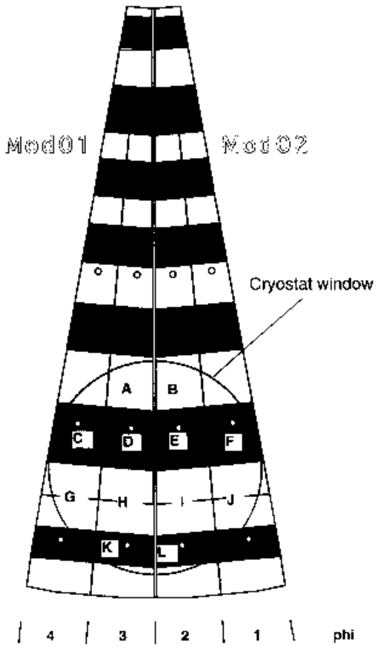

Figure 4: The geometric layout of impact positions D, E, H, & I on the front face of HEC modules Zero.

slices occur before the signal rise, while the signal maximum occurs in the 8th time slice. The energy deposited in each cell is reconstructed from the signal maximum which can be determined by a variety of methods described in section 5.1.1.

The pedestals for each cell are determined from the first four time slices averaged over all events within the run [4], as shown in Figure 5. On an event by event basis the average of the first 4 time slices is observed to be stable over the duration of a run.

4 Electron Energy Scans

4.1 Energy Reconstruction

The electron sample is isolated by applying trigger cuts and a signal shape cut. Electron energies are then reconstructed by summing the energy deposited in a predefined cluster and applying a global electromagnetic scale factor, $\alpha_{\rm em}$.

[4]The use of run pedestals in lieu of event pedestals (defined as the average of the first 4 time slices for each event) provides higher statistics and hence a more precise knowledge of the pedestals for each cell. In fact, the use of event pedestals affects a considerable degradation of the calorimeter resolution.

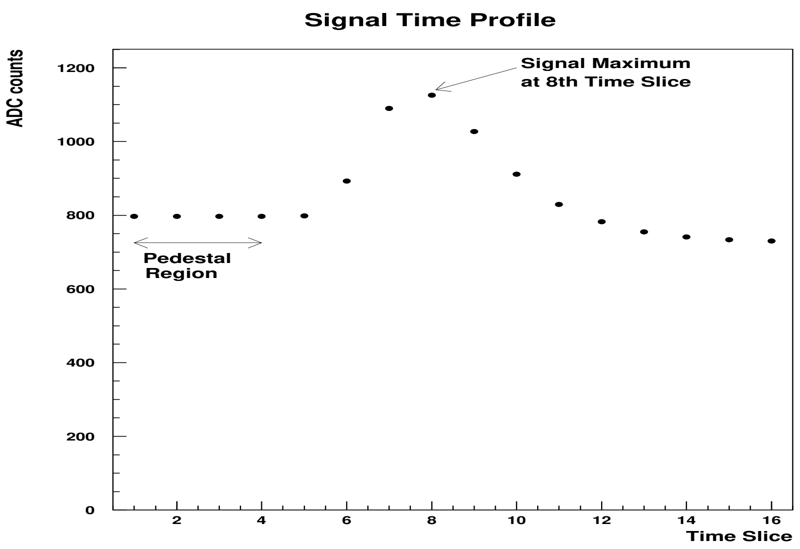

Figure 5: Sample signal time profile (average signal for run 7355, 180 GeV pions, impact position D) showing the pedestal region (time slices 1-4) and the signal maximum which typically occurs at time slice 8.

4.1.1 Trigger Cuts

Events from the electron data are selected by requiring that the following trigger logic be satisfied:

$$pretrigger \bullet \overline{halo} \bullet \overline{muon} \bullet \overline{pileup} \bullet \overline{random} \tag{1}$$

where

$$pretrigger = B1 \bullet F1 \bullet F2, \quad halo = VM + hole, \quad muon = M1 \bullet M2, \tag{2}$$

pileup is true when a second trigger coincides with the first, and *random* is true when the data acquisition system has requested a random trigger of any sort (hardware or software). Refer to Figure 1 for the locations of the various detectors in the testbeam setup. $B1$ is a scintillating detector upstream from the cryostat where the beam leaves the beam pipe after being bent by the last dipole magnet, Bend9. $F1$ and $F2$ are scintillating detectors which are oriented perpendicular to one another and effectively define the transverse size of the beam for triggered events. They are mounted on a motorized table (y-table) which can be displaced in the vertical direction. VM is a plane of scintillating detectors located close to the front of the cryostat with an aperture in the center coinciding with the cryostat window. *hole* is a scintillating detector mounted on the y-table with a small aperture in its center. $M1$ and $M2$ each form a plane of scintillating detectors behind the cryostat for muon identification. Čerenkov detectors are not employed to isolate electrons from pions.

4.1.2 Signal Shape Cut

The trigger cuts are not sufficient to properly veto low energy background events. A signal shape cut is used to further isolate the electron sample.

For each impact position a "subcluster" is defined which consists of 3 cells: the impact cell and the two cells lying directly behind it in the second depth within the same ϕ segmentation. A minimum of one of these 3 "subcluster" cells is required to have a signal shape consistent with energy deposition in that cell [5]: a maximum between the seventh and ninth time slices with the signal decreasing everywhere in the vicinity of the maximum, where the vicinity is defined as the surrounding seven time slices. There are no requirements on the amplitude of this signal. Approximately 3500 electron events satisfy the combined trigger and signal shape cuts for each data run.

4.1.3 Clustering

The energy of the incident electrons is reconstructed by summing the individual energies deposited in a cluster of 3 cells after applying hardware calibration constants. The cluster size and shape have been chosen so as to minimize the energy resolution, and coincide exactly (in the electron case) with the cells chosen for the "subcluster" described above. Figure 6 shows the clusters chosen for the 4 impact positions.

The energy deposited in each cluster is histogrammed and a Gaussian curve is fit to the data in a 3σ range about the mean for each run. Histograms and fits for a representative impact position (D) are shown in Figure 7.

4.1.4 Global Electromagnetic Scale, α_{em}

A single constant, α_{em}, is used to convert the energies from nA to GeV. This global electromagnetic scale is determined for each impact position by minimizing the following function:

$$\chi^2 = \sum_{\mathrm{i}}^{\mathrm{runs}} \frac{\left(\alpha_{\mathrm{em}} \left\langle E_{\mathrm{cl,i}}(\mathrm{nA})\right\rangle - E_{0,i}\right)^2}{\sigma_i^2} \tag{3}$$

where σ_i are in GeV and are iteratively adjusted, $E_{\mathrm{cl}}(\mathrm{nA})$ is the mean energy arrived at by fitting Gaussian curves to the energy distributions as described in section 4.1.3, and E_0 is the nominal beam energy expressed in GeV.

The global electromagnetic scale is found to be similar at all impact points. The average over all 4 impact positions is:

$$\alpha_{\mathrm{em}} = 0.112 \text{ GeV/adc} = 3.41 \text{ GeV}/\mu\text{A}. \tag{4}$$

[5] see [3] for a description of the signal shape analysis package

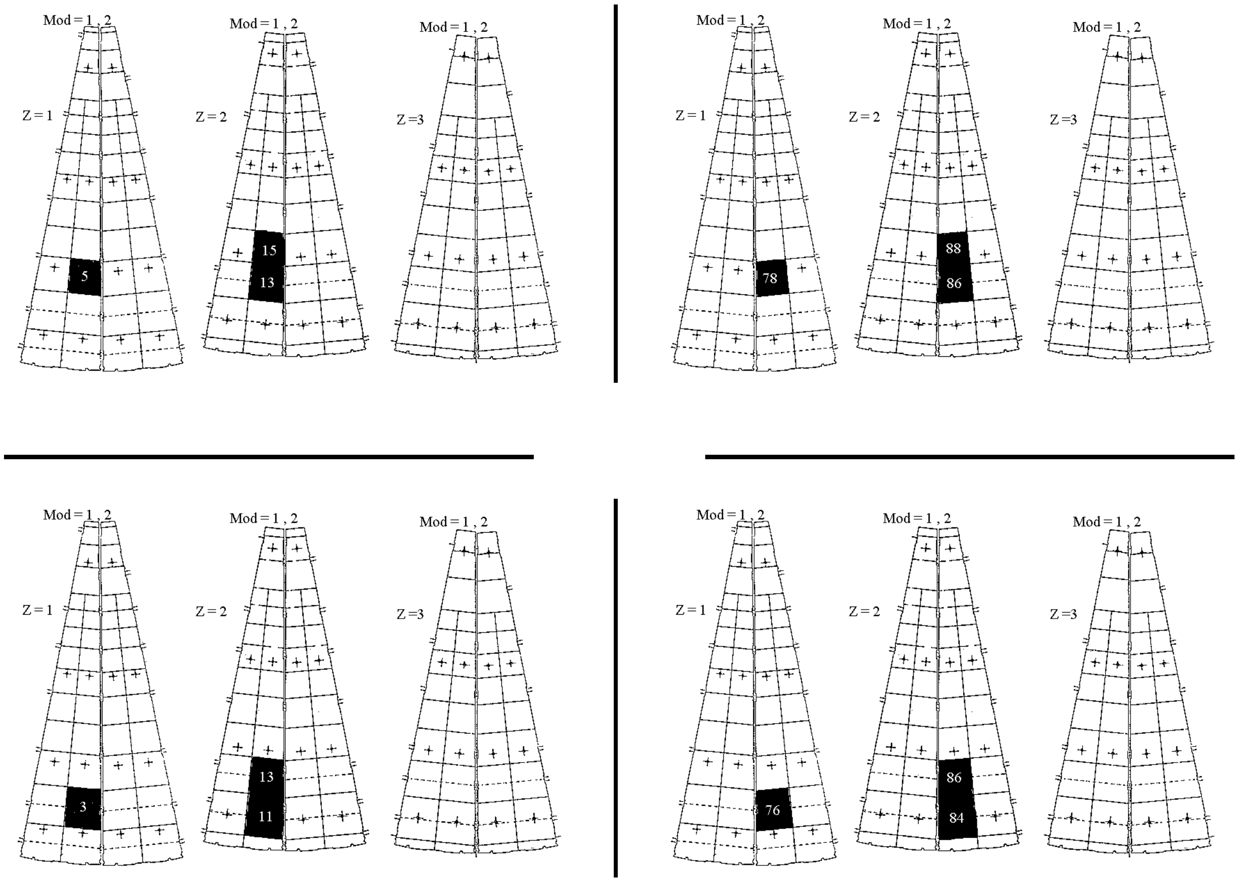

Figure 6: Map of cells used in electron clusters: points D, E, I, H (clockwise from top left).

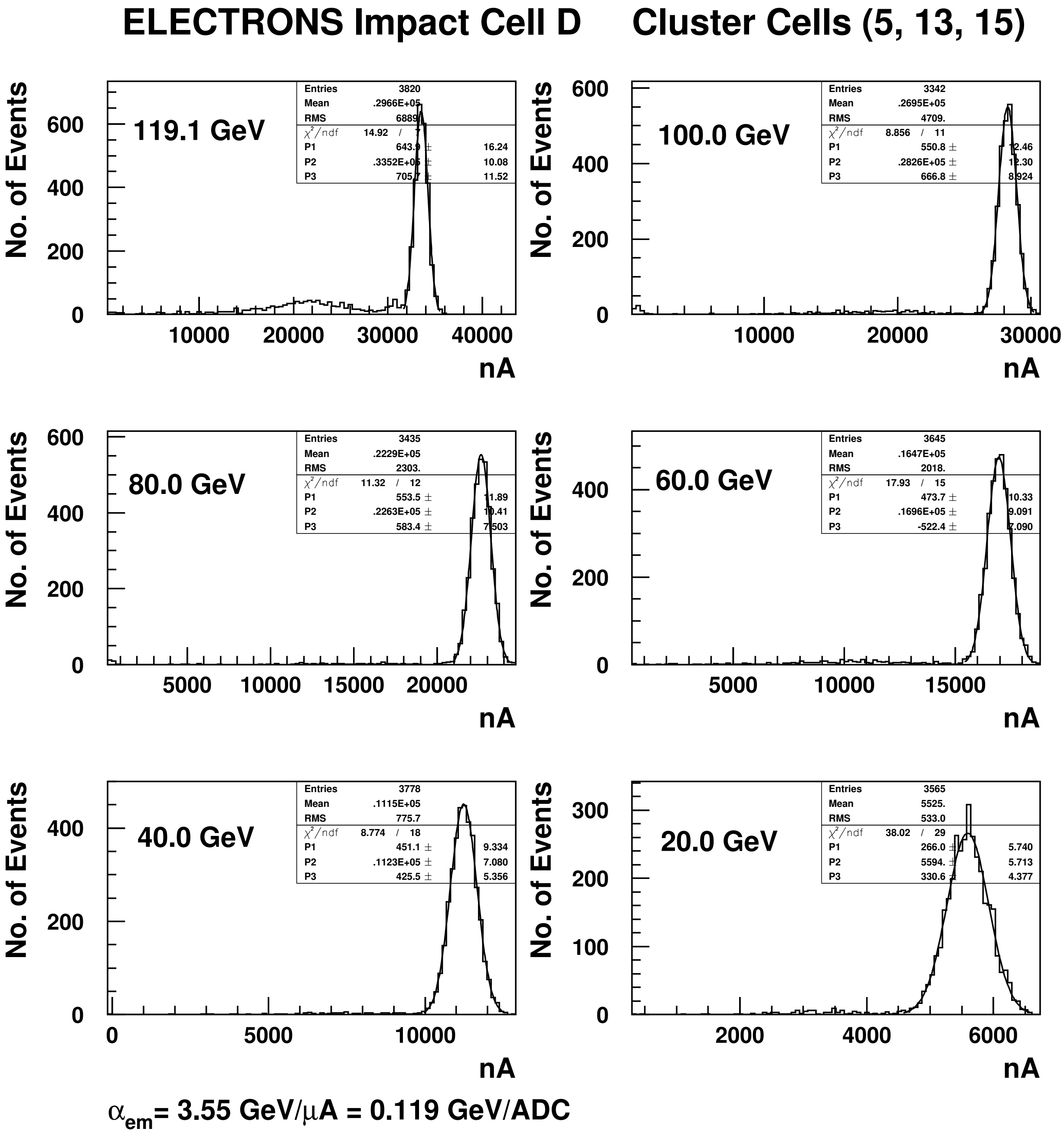

Figure 7: Electron cluster energy (calibrated data) for a typical impact point(D).

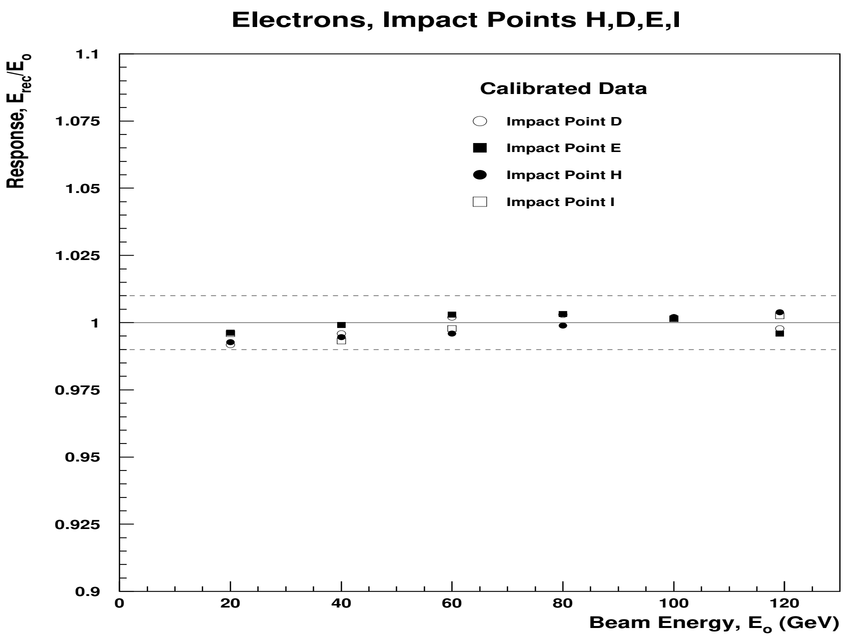

Figure 8: Electron response of calorimeter vs. beam energy.

4.2 Response

By applying α_{em} to the fit mean energy for each run, a response curve is obtained, Figure 8. The response is linear to within 1% over all impact positions. The response linearity is improved by the hardware calibration.

4.3 Resolution

The energy resolution σ/E is plotted versus the beam energy in Figure 9. The resolution of the calorimeter is parameterized as:

$$\frac{\sigma}{E} = \frac{A}{\sqrt{E_0}} \oplus B \oplus \frac{C}{E_0}, \tag{5}$$

where A is the sampling term, B is the constant term, and C is the electronic noise term. The results of the fit for each impact position with all three parameters left free are:

Position	A(%GeV$^{\frac{1}{2}}$)	B(%)	C(GeV)
Module 1			
D	21.2 ± 1.1	0.7 ± 0.3	0.69 ± 0.08
H	22.7 ± 0.5	0.0 ± 1.5	0.50 ± 0.07
Module 2			
E	20.9 ± 0.9	0.7 ± 0.2	0.60 ± 0.07
I	22.8 ± 0.3	0.0 ± 0.4	0.44 ± 0.06

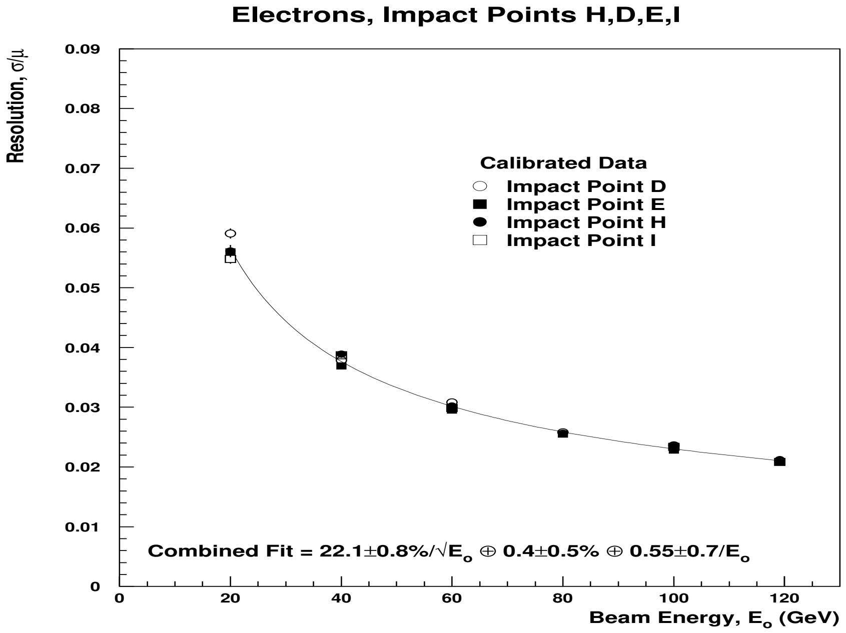

Figure 9: Electron energy resolution with 3 free parameters.

The results are consistent over all impact positions. A combined fit produces the following results:

$$\frac{\sigma}{E} = \frac{22.1 \pm 0.8\%}{\sqrt{E_0}} \oplus 0.4 \pm 0.5\% \oplus \frac{0.55 \pm 0.07}{E_0}, \qquad \frac{\chi^2}{\mathrm{DoF}} = 2.03 \tag{6}$$

where E_0 is expressed in GeV.

The noise term is consistent with noise measurements made from random trigger events (described in section 5.1.4).

5 Pion Energy Scans

5.1 Energy Reconstruction

5.1.1 Signal Reconstruction

Since the standard HEC testbeam readout contains 16 time slices for each channel for each event, it is necessary to define a method for reconstructing the maximum signal. In this analysis, two different methods of signal reconstruction are compared. The first is a simple cubic fit to 4 time slices near the maximum. This is one of the methods available in the *hec_adc* testbeam software package and is described in detail in [3]. The second method, also available in the *hec_adc* package, uses a digital filtering technique to perform the reconstruction. This technique, as explained in references [4, 5], uses the autocorrelation function of the time slices to maximize the signal/noise ratio for determination of the time origin and amplitude of the signal.

5.1.2 Clustering

Once the signal is reconstructed in each cell, the energy of a pion is defined by the sum[6] of the signals in a cluster of cells. Clusters as small as 10 cells and as large as 40 cells have been evaluated; a detailed comparison of the energy resolution resulting from each cluster is shown in section 5.2.2. Minimization of the overall energy resolution is the criteria for choosing a cluster size. Unless otherwise stated, the cluster size presented herein is 19 cells (18 for point I) with the cluster geometry illustrated in Figure 10 for each impact position.

The cells in these clusters were chosen by evaluating the average energy content of each cell, not by geometric considerations. However, Figure 10 shows that, as expected, the clusters are all similar in geometric layout.

5.1.3 Pion Sample

In order to remove impurities in the pion sample (eg. muons), several trigger cuts are used. These cuts have been described in detail for the electron analysis (section 4.1.4) and include a physics trigger requirement, a muon veto, and a subcluster cut. The energy distributions with cuts applied are shown in Figure 11 for 4 beam energies from a representative energy scan (position H). The number of pion events satisfying these cuts ranges from approximately 3000 to 8000 for the 40 to 180 GeV runs, and 168 to 260 events for the 20 GeV runs.

5.1.4 Resolution Optimization Techniques

The fractions of electromagnetic and hadronic energies in a pion shower vary with beam energy. Since our calorimeter is intrinsically non-compensating, depth weights that vary with energy are employed to evaluate the energy resolution and response of the calorimeter to pions.

In this analysis, two steps were taken in order to obtain the depth weights. First, an overall (global) hadronic scale is calculated over all energies by minimizing the following function:

$$\chi^2 = \sum_{\mathrm{i}}^{\mathrm{runs}} \frac{\left(\alpha_{\mathrm{had}} \left\langle E_{\mathrm{cl},i}(\mathrm{nA}) \right\rangle - E_{0,i}\right)^2}{\sigma_i^2} \tag{7}$$

where α_{had} is the global hadronic scale, $E_{0,i}$ is the beam energy, σ_i refers to the resolution at each energy and $\left\langle E_{\mathrm{cl},i}(\mathrm{nA}) \right\rangle$ refers to the average energy obtained from a Gaussian fit on the energy distribution of a particular point. This is necessary only to set a convenient scale for the analysis, the value of α_{had} does not affect the resolution results. After this scale is

[6] This need not be a simple sum. As described in section 5.1.4, weights may be applied to optimize the resolution.

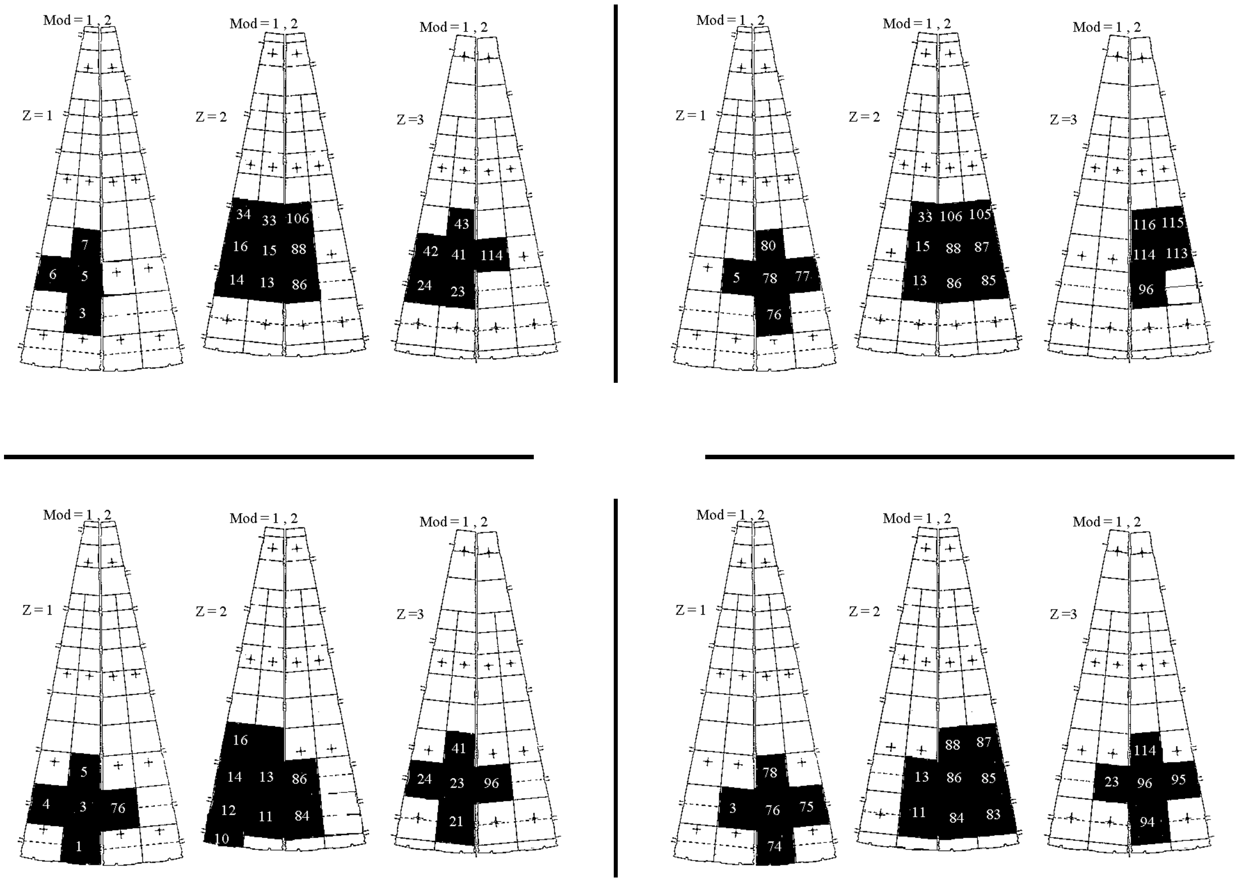

Figure 10: Map of cells used in pion clusters: points D, E, I, H (clockwise from top left).

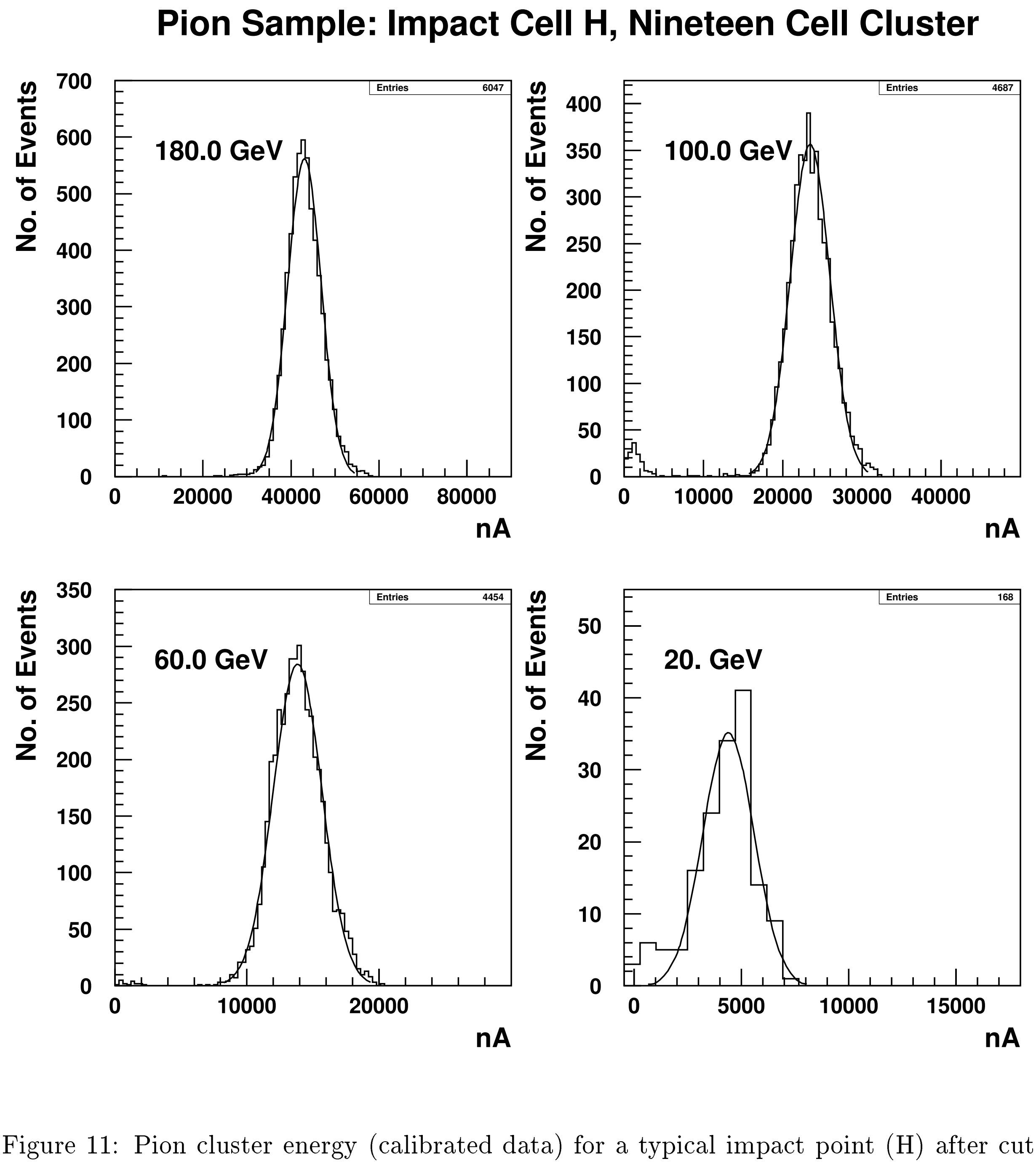

Figure 11: Pion cluster energy (calibrated data) for a typical impact point (H) after cuts, beam energies 180 to 20 GeV. Depth weighting is not employed in producing these histograms except for a factor of 2 in the back depth to account for the change in sampling fraction.

obtained, the depth weights, c_z, for each energy are found by minimizing

$$\frac{1}{\sigma^2}\sum_{\text{events}}\left(\alpha_{\text{had}}\sum_z c_z E^z_{\text{cl}}(\text{nA}) - E_0\right)^2. \tag{8}$$

Due to the differing sampling fractions in the front and back wheels of the calorimeter, a factor of two is expected to appear in the weight of the third depth relative to the first two. This expectation is slightly modified in module 2 due to the high voltage problems in some sub-gaps in the back wheel. This should produce an increase in the depth weights in the rear wheel of module 2 with respect to module 1 to compensate for the loss of signal.

Energy distributions for a representative energy scan (position H) are shown in Figures 12 & 13 after depth weights have been applied for a 19 cell cluster. The Gaussian shape of these histograms degrades with increasing energy indicating energy leakage out of the cluster at high energies. This effect can be reduced by using a larger cluster size such as a 40 cell cluster, as shown in Figure 14. However, the resolution does not differ for the two cluster sizes at high energy as shown in Figure 17. A comparison of the effect of cluster size on resolution and response is presented in section 5.2.2.

Once the depth weights have been found and applied to the cluster, the energy resolution of the calorimeter can be evaluated. To express the energy resolution of the Hadronic Endcap over an energy range the standard parameterization is

$$\frac{\sigma}{E} = \frac{A}{\sqrt{E_0}} \oplus B \oplus \frac{C}{E_0} \tag{9}$$

where A is interpreted as a sampling term, B as a constant term and C as a noise term. For electromagnetic showers this is an accepted parameterization of the resolution for which the interpretation of the three parameters as sampling, constant and noise terms is well understood. For hadronic showers this parameterization is less sound. Other parameterizations have been proposed [6], but the electromagnetic resolution formula is widely used to express hadronic energy resolutions. The three terms in the resolution can be highly correlated, thus making the interpretation of terms difficult. One way to reduce the correlation effects is to independently calculate the noise term and remove it from the fit. The noise at each energy can be calculated by adding the noise of each cell in the cluster taking into account all cell to cell correlations or it can be measured directly from random trigger events within the run or from dedicated noise runs.

In this analysis, the noise is measured from random trigger events within each run after applying the energy dependent depth weights obtained from Equation 8. The use of energy dependent depth weights means the noise term is no longer independent of energy for a given cluster. Having measured the energy dependent noise, it is subtracted in quadrature from the resolution for each run and a two parameter fit is performed.

5.2 Signal Reconstruction and Clustering Techniques

The effects of different signal reconstruction methods and cluster sizes have been evaluated by comparing the pion energy resolution and response of the calorimeter for a single impact position (H).

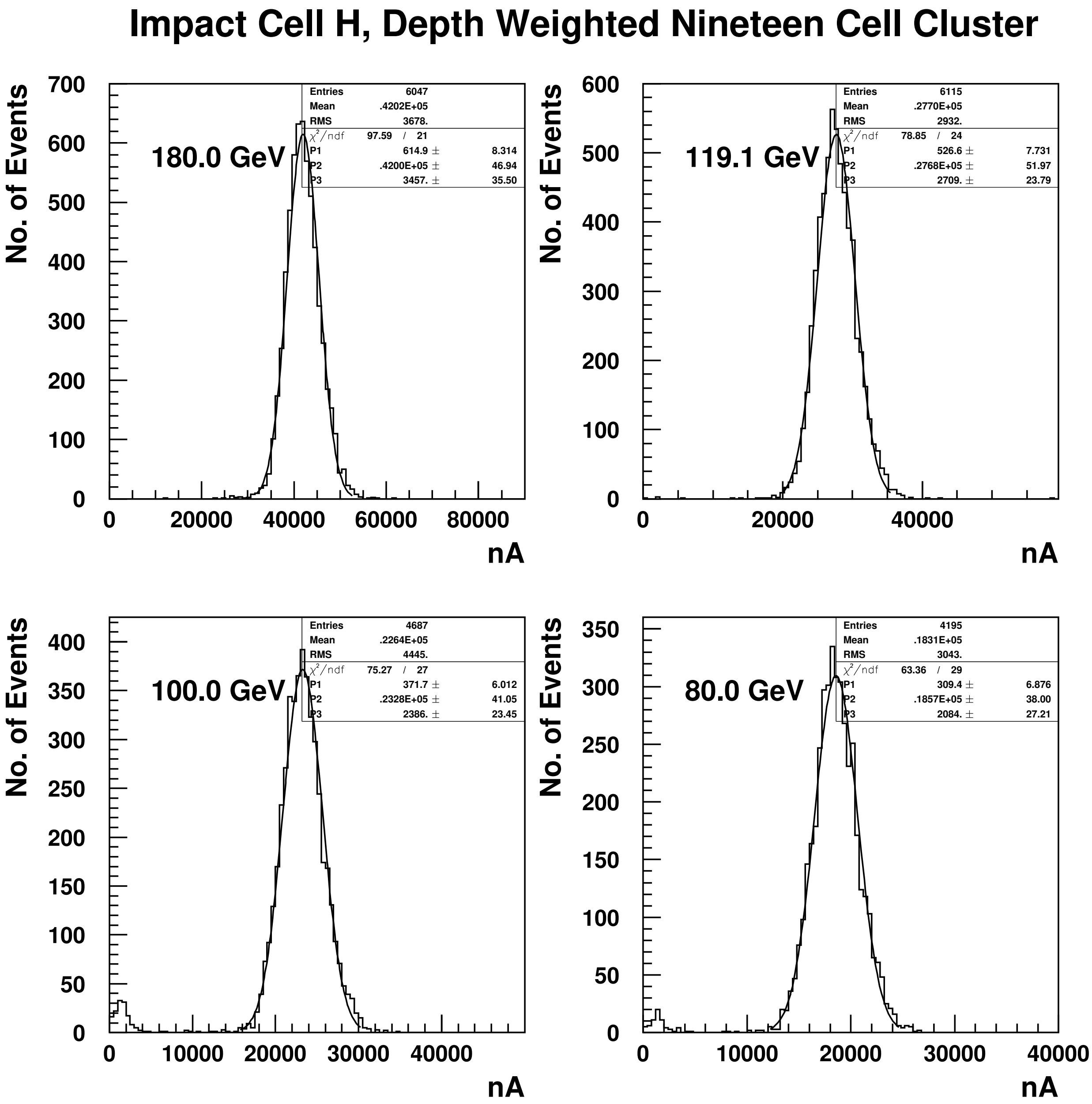

Figure 12: Pion cluster energy (calibrated data) for a typical impact point (H) after cuts and depth weighting, beam energies 180 to 80 GeV.

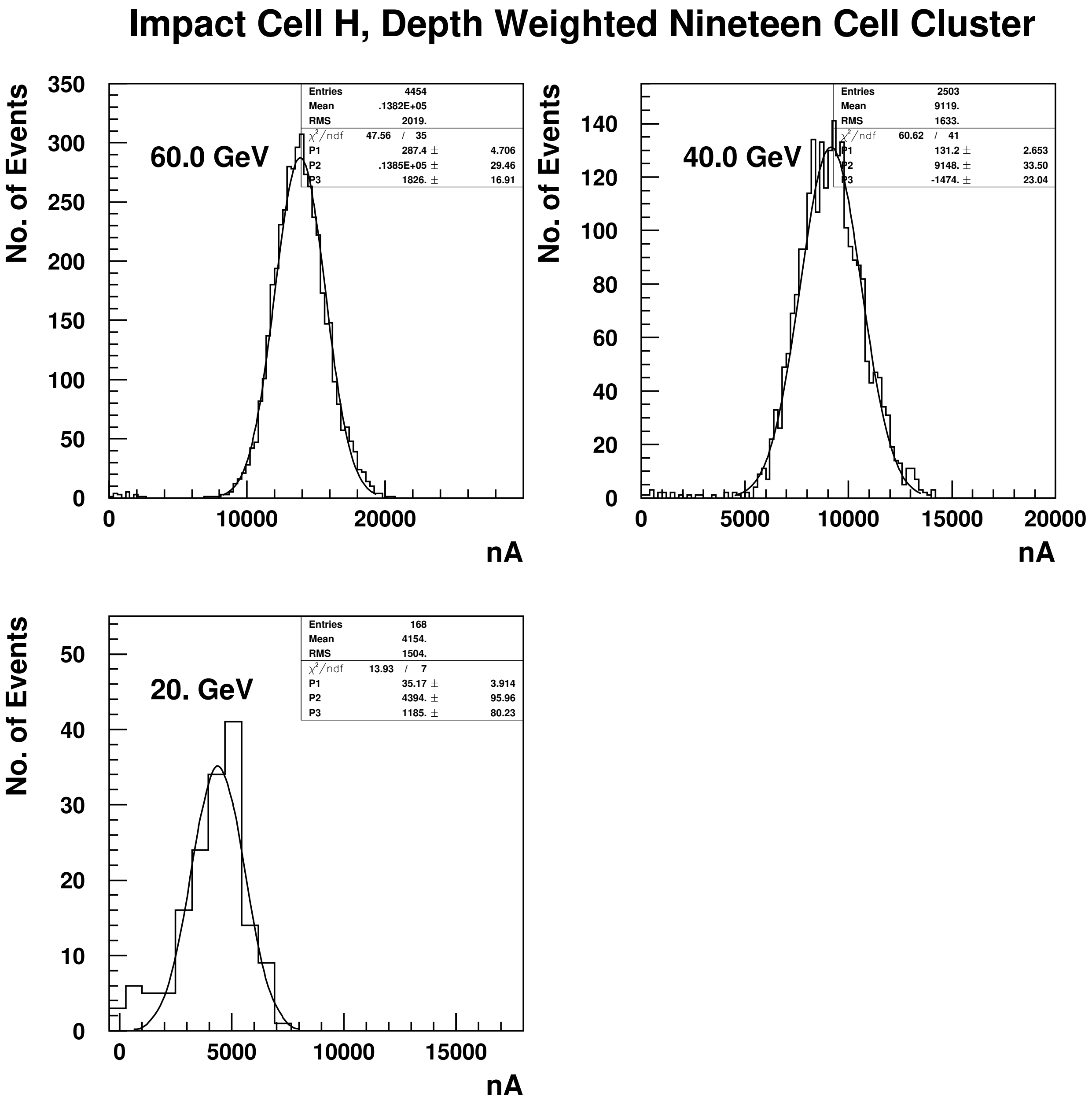

Figure 13: Pion cluster energy (calibrated data) for a typical impact point (H) after cuts and depth weighting, beam energies 60 to 20 GeV.

5.2.1 Comparison of Cubic Fit and Digital Filtering

As described in section 5.1.1, there are several different ways to reconstruct the signal amplitude in each cell. For all impact positions two methods have been compared in detail: cubic fit and digital filtering.

The calorimeter's response to pions has been evaluated with respect to the two different methods. Figure 15 shows the pion energy response of the calorimeter for both cubic fit and digital filtering signal reconstruction. This figure shows that the response for cubic fit varies significantly more than it does for digital filtering over the studied energy range.

The effect of the different signal reconstruction methods on energy resolution is also evaluated. Figure 16 shows a comparison of the resolution for both methods for impact position H. At energies $\geq$ 120 GeV the two methods produce similar results. However, at energies from 20 to 100 GeV the cubic fit results are inferior. The cubic fit method tends to overestimate the energy in cells with low signals and thus, when the signal in a particular cell is low, a systematic high-energy bias is produced. When the cubic fit is used to reconstruct zero energy signals from random trigger events it will measure above zero average energies in each cell, a clear indication of this bias. This version of the cubic fit algorithm uses a special treatment of low-signal cells in an attempt to address this problem. If the signal falls below 10 times the pedestal rms of the cell, the 8th time slice is used instead of a cubic fit to four time slices. This helps to reduce the bias, but still leads to worse resolution than digital filtering at low energies. Due to these effects, digital filtering has been chosen as the preferred signal reconstruction method and the remainder of the results presented here are obtained using this method[7].

5.2.2 Effect of Cluster Size on Resolution

The number of cells used in a cluster influences the measured energy resolution of the calorimeter. A very small cluster may exclude a significant fraction of the pion energy, effectively creating leakage and degrading the resolution, particularly the sampling and constant terms. The advantage of a small cluster is that, by including fewer cells, the electronic noise is reduced. In ATLAS smaller clusters might be necessary to separate close-together jets. A large cluster reduces problems associated with leakage, limited by real leakage from the calorimeter, but includes many cells and hence an increased electronic noise contribution. A compromise must be made which finds the optimum overall resolution while using realistic cluster sizes.

Figure 17 shows a comparison of energy resolution for 4 different cluster sizes for position H. These clusters range from a small cluster of 10 cells to a large 40 cell cluster. The results show that the best overall resolution is obtained by a cluster containing 18-19 cells at all beam energies. Larger clusters than 19 cells do not improve the energy resolution at high energies, implying that leakage from the cluster is minimal. Small clusters (eg. 10 cells) do not improve the resolution at low energies where the noise term takes on added significance.

[7]For four channels (94,95,114,116) for which digital filtering weights did not exist, cubic fit was used.

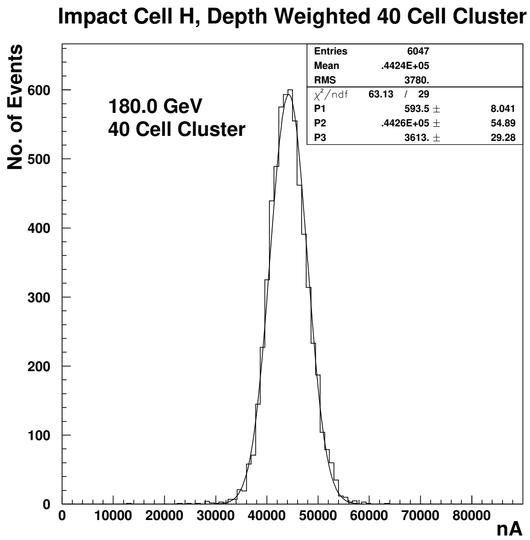

Figure 14: Pion cluster energy distribution for impact point H after cuts and depth weighting for a 40 cell cluster, beam energy 180 GeV. Note the improvement in the Gaussian fit over that presented for a 19 cell cluster in Figure 12.

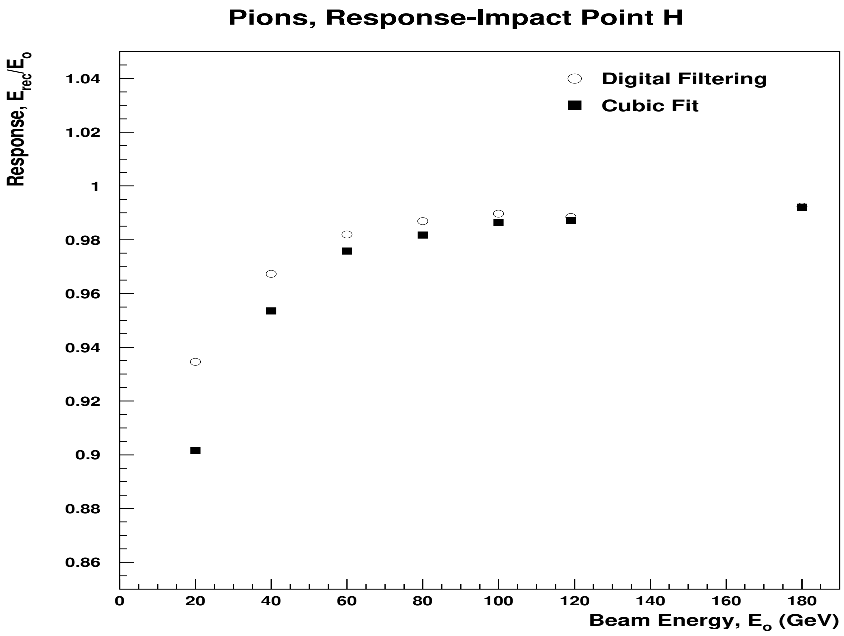

Figure 15: Comparison of cubic fit and digital filtering response for pions.

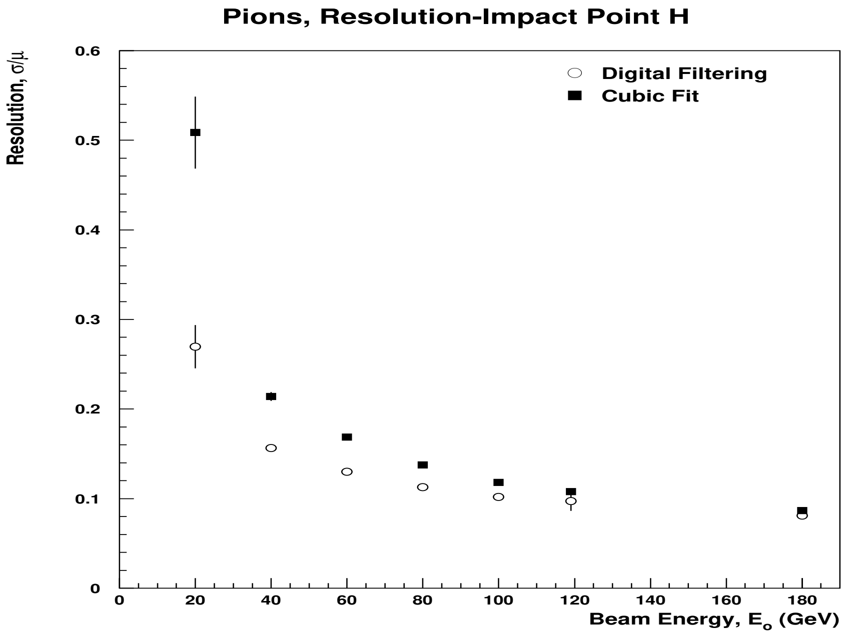

Figure 16: Comparison of cubic fit and digital filtering resolution for pions.

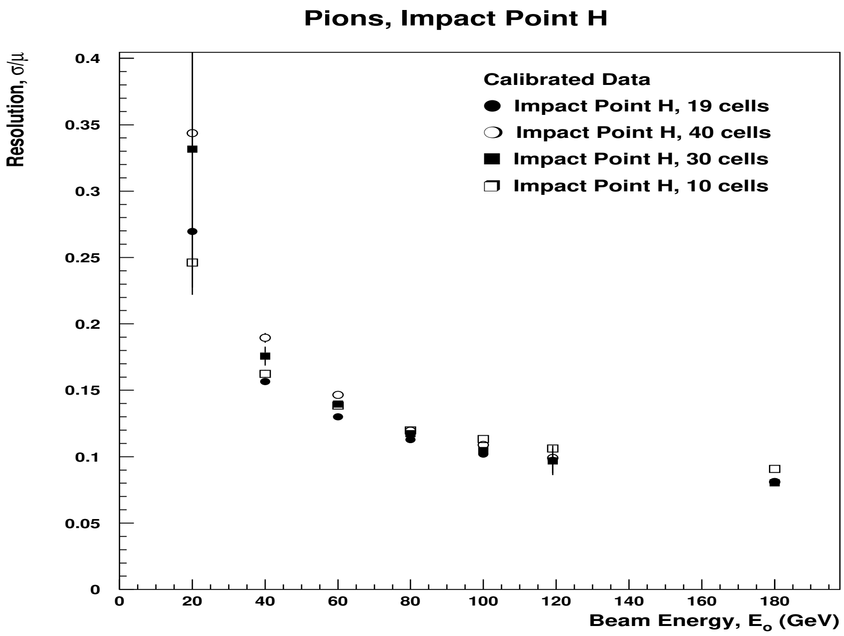

Figure 17: Comparison of energy resolution for four different cluster sizes for pions at position H.

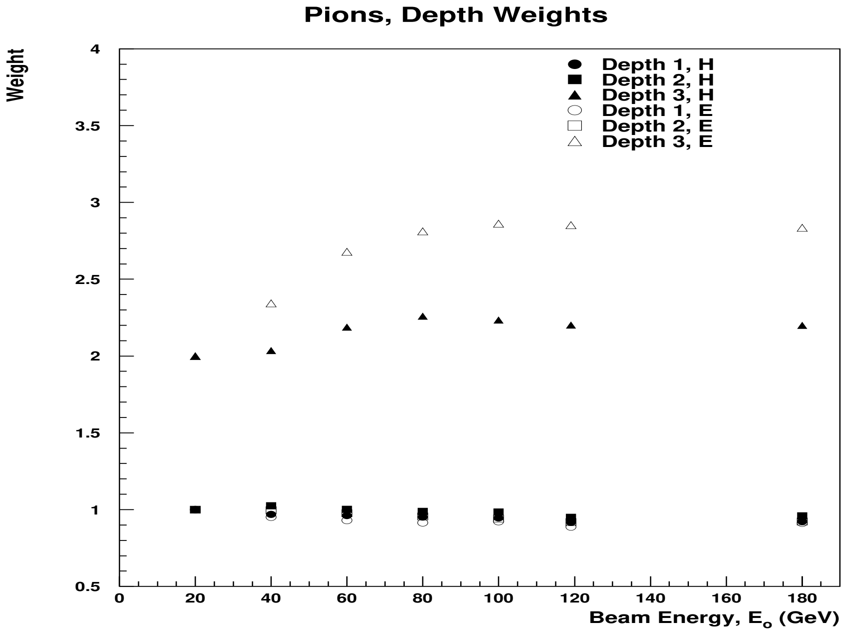

Figure 18: Depth weights are shown for impact position D and E (affected by HV problems).

5.3 Resolution and Response for Different Impact Positions

The resolution and response analysis is performed at 4 different impact positions. Two of these impact positions (E and I) are affected by the high voltage problems in module 2. This leads to different depth weights for these two positions compared to the other two positions (H and D). A comparison of the depth weights obtained for impact points H and E are presented in Figure 18. This shows that the weights for the first two depths are in agreement for the two positions, however, the weight of the third depth is higher by approximately a factor of 4/3 for pad E. This factor precisely matches expectation as it is compensating for a loss of 1/4 of the signal deposited in the third depth. Once these weights have been used to correct for the signal loss in module 2, the response and resolution can be compared.

Figure 19 shows the calorimeter response to pions at the four impact positions. From this figure it can be seen that the response is consistent over all impact points.

The resolution, measured at all four impact positions is shown in Figure 20. This figure illustrates the consistency between impact points despite the high voltage problems in one of the modules. The adjustment of the depth weights effectively compensates for the loss of signal.

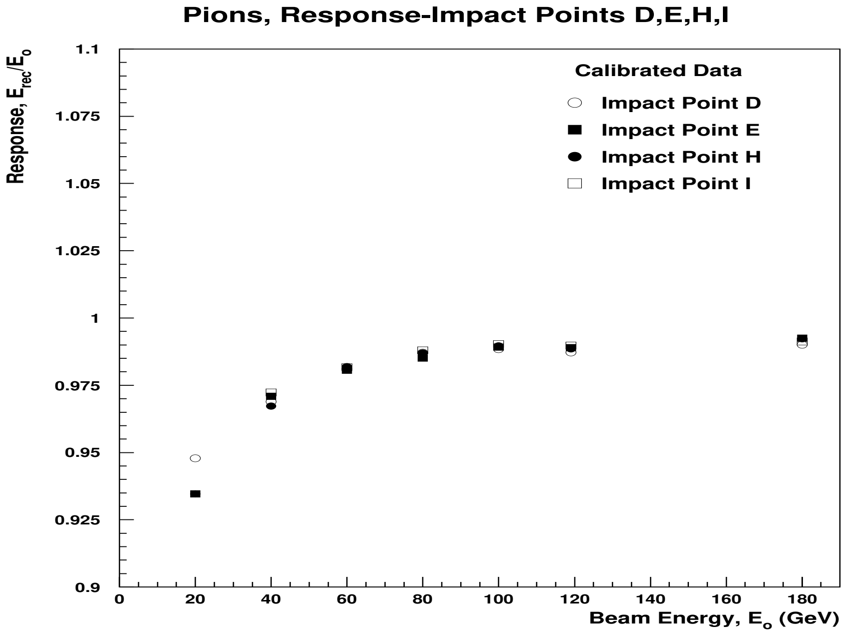

Figure 19: Pion response is compared for four impact positions.

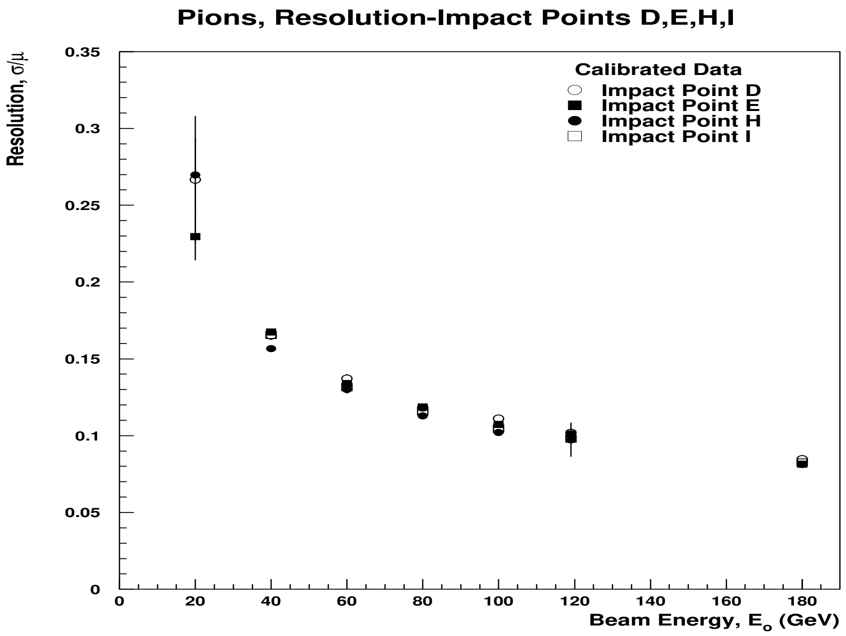

Figure 20: Resolution is compared for four impact positions.

5.4 Overall Resolution and Response

As discussed in section 5.1.1, in order to parameterize the pion energy resolution of the calorimeter, a two parameter fit is used (the first two parameters of equation 9). The third parameter, known as the noise term, can be measured directly by applying the depth weights obtained from physics events to random trigger events. The noise is then subtracted (in quadrature) before the fit is made. Measured values of the noise for 18-19 cell clusters are shown in the table below.

Energy (GeV)	Position D Noise (GeV)	Position E Noise (GeV)	Position H Noise (GeV)	Position I Noise (GeV)
20	3.4	2.9	3.2	n/a
40	3.6	3.4	3.3	3.7
60	3.9	3.8	3.5	4.1
80	4.0	3.8	3.5	3.9
100	4.0	4.2	3.4	4.5
120	3.8	4.0	3.6	4.6
180	4.7	4.3	3.4	4.1

The errors in the noise range from 0.1 to 0.3 GeV. With errors taken into account, the measured noise is not constant with varying energy or impact position. This behaviour is expected as the noise depends on energy through the energy dependent depth weights and depends on impact position due to the different cells used in each cluster.

The energy resolution σ/E is plotted (after subtracting in quadrature the electronic noise terms) versus the beam energy in Figure 21. A two parameter fit is performed over the points from all impact positions. The results of the fit for each impact position are:

Position	A(% GeV$^{\frac{1}{2}}$)	B(%)	χ^2/DoF
Module 1			
D	81 ± 4	6.0 ± 0.5	1.08
H	80 ± 2	5.3 ± 0.4	0.43
Module 2			
E	86 ± 2	4.9 ± 0.4	1.80
I	80 ± 3	5.2 ± 0.3	0.25

A combined fit is superimposed on Figure 21. This fit yields (E_0 in GeV)

$$\frac{\sigma}{E} = \frac{82 \pm 1\%}{\sqrt{E_o}} \oplus 5.2 \pm 0.2\%, \qquad \frac{\chi^2}{\text{DoF}} = 1.60. \tag{10}$$

6 Conclusions

The Hadronic Endcap modules Zero were successfully tested in April 1998. The performance at all four impact positions studied are comparable after the application of depth weights to compensate for high voltage problems in module 2.

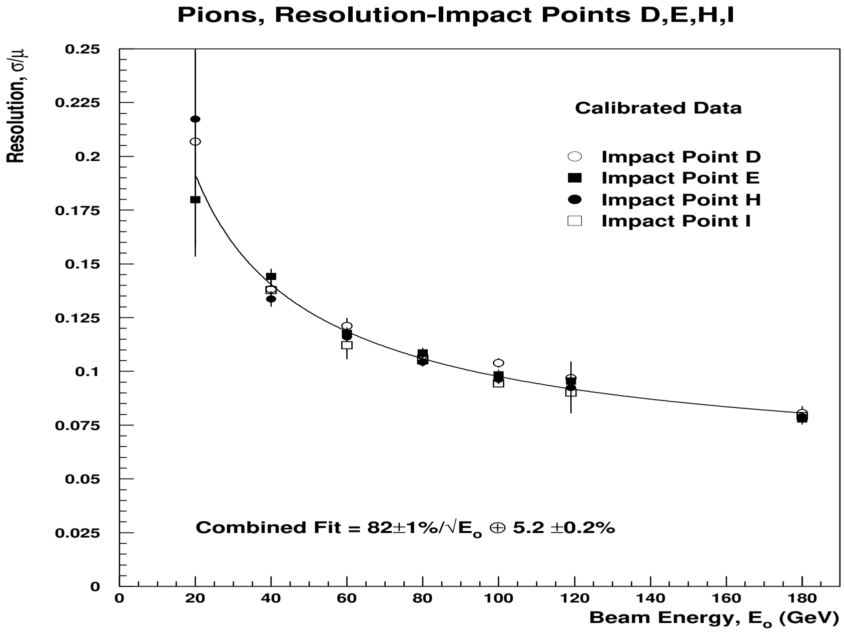

Figure 21: Resolution is compared for four impact positions after pre-subtraction of noise. A combined fit is superimposed. (E_o is in GeV)

The use of digital filtering for signal reconstruction affects an improvement in response and resolution over a simple cubic fit.

Using a 3 cell cluster, the response to electrons is found to be constant to within 1%. A combined fit over all impact positions produces the following parameterization for the energy resolution (E_o in GeV):

$$\frac{\sigma}{E} = \frac{22.1 \pm 0.8\%}{\sqrt{E_o}} \oplus 0.4 \pm 0.5\% \oplus \frac{0.55 \pm 0.07}{E_o}.$$

An 18-19 cell cluster is the optimum cluster size for reconstructing the pion energy. The response to pions is found to be linear within 6%. After pre-subtracting the electronic noise in quadrature, the energy resolution is parameterized as (E_o in GeV):

$$\frac{\sigma}{E} = \frac{82 \pm 1\%}{\sqrt{E_o}} \oplus 5.2 \pm 0.2\%.$$

7 Acknowledgments

The authors would like to thank Andrei Minaenko for many useful discussions.

References

[1] ATLAS Collaboration, *ATLAS Liquid Argon Technical Design Report*, December 15, 1996.

[2] ATLAS - HEC Collaboration, “Electron and Pion Test Beam Data Analysis of the Hadronic Endcap Prototype Calorimeter”, *ATLAS Liquid Argon Note No. 95*, April 16, 1998.

[3] Lefebvre, M. and O’Neil, D., “The HEC Testbeam Offline Software: The hec_adc Package”, *ATLAS LAr Note - in progress*. Refer to `http://wwwhep.phys.uvic.ca/~uvatlas/hec_adc/hec_adc.html`.

[4] Cleland, W.E. and Stern, E.G., “Signal processing considerations for liquid ionization calorimeters in a high rate environment”, *Nuclear Instruments and Methods in Physics Research*, A 338(1994) 467-497.

[5] Kurchaninov, L., Levitsky, M., “Optimal Weighting of signal Samples for LAr Calorimeters”, *ATLAS Liquid Argon Note No. 44*, July 14, 1996.

[6] Groom, Don, “What really goes on in a hadron calorimeter?”, presented at *VII International Conference on Calorimetry in High Energy Physics* at the University of Arizona, Tucson, Arizona, November 9-14, 1997. Refer to `http://pdg.lbl.gov/~deg/calor97.html`.

Appendix: Data Samples

Electron Data				
Energy (GeV)	point D Run #	point E Run #	point H Run #	point I Run #
20	7353	7350	7352	7351
40	7298	7291	7295	7294
60	7255	7259	7253	7260
80	7299	7311	7303	
100	7334	7341	7330	7342
119.1	7065	7088	7071	7079
Pion Data				
Energy (GeV)	point D Run #	point E Run #	point H Run #	point I Run #
20	7354	7371	7369	
40	7297	7292	7296	7293
60	7281	7287	7280	7285
80	7300	7312	7304	7310
100	7335	7340	7331	7343
119.1	7196	7154	7182	7146
180	7355	7359	7356	7360